Received: 1 March 2022 | Revised: 10 June 2022 | Accepted: 29 June 2022

DOI: 10.1002/er.8370

RESEARCH ARTICLE

INTERNATIONAL JOURNAL OF ENERGY RESEARCH WILEY

Computational investigation of auto-thermal reforming process of diesel for production of hydrogen for PEM fuel cell applications

Dimitrij Ješić[1] | **Vivian Erklavec Zajec**[1] | **David Bajec**[1] | **Gregor Dolanc**[2] | **Gorazd Berčič**[1] | **Blaž Likozar**[1]

[1]Department of Catalysis and Chemical Reaction Engineering, National Institute of Chemistry, Ljubljana, Slovenia

[2]Department of Systems and Control, Jozef Stefan Institute, Ljubljana, Slovenia

Correspondence
Blaž Likozar, Department of Catalysis and Chemical Reaction Engineering, National Institute of Chemistry, Hajdrihova 19, 1001, Ljubljana, Slovenia.
Email: blaz.likozar@ki.si

Funding information
Javna agencija za raziskovalno dejavnost RS, Grant/Award Numbers: J2-1724, P2-0152; European Defence Agency, Grant/Award Number: B1490GEM3GP

Summary

Hydrogen for the use in electrochemical fuel cells (FCs) can be obtained from diesel's sourced energy. A small scale process of the catalytic auto-thermal reforming (ATR) with the operational water-gas shift (WGS) for the production of hydrogen with suitable purity grade as a resource in the high temperature polymer membrane redox FCs (HT-PEMFCs) for auxiliary power systems was proposed. The reactors for hydrocarbon ATR dehydrogenation reactions, WGS processor serial treatment and downstream were designed. Technology was simulated using Aspen Plus software. Gibbs minimization was applied to validate the product compound composition for both units' yields, modelling was analysed, and the heat at the ATR device fluid inlet, the potential of pressure, feed, the influence of the oxygen to carbon (C) amount ratio, and the steam to total indicated C equivalent were investigated. one dimensional models were used for ATR/WGS. The first was considered as a plug flow, while the latter as packed-bed vessel. Particular kinetic parameters were estimated from literature; other functional conditions were specified. Combined sequential results, assessed from calculations, allow for a successful engineered construction, operation and intensification of ATR, which requires a good physical understanding, but also control of thermodynamic equilibria, transport phenomena and mechanistic chemical rates.

KEYWORDS

autothermal reforming, fuel cell, hydrogen, modeling, water gas shift

1 | INTRODUCTION

Hydrocarbon fuels can be efficient hydrogen carriers mainly due to their high hydrogen density and existing infrastructure. Extensive studies have been conducted on the use of hydrocarbon fuels as hydrogen sources for fuel cell applications, particularly gasoline, diesel[1-4] and jet fuel.[5-7] The major drawback of these technologies is that they have difficulties in maintaining high thermal efficiency and low fuel consumption while reducing

emissions such as CO and CO_2.[8,9] Research is placing great emphasis on finding cleaner and more efficient designs.[2]

Various ways of producing hydrogen from hydrocarbons have been studied: carbon dioxide reforming,[10-12] partial oxidation of hydrocarbons,[13,14] steam reforming[15-18] and technologies combining different aspects,[2,19-21] such as autothermal reactors. The latter was originally proposed by Argonne National Laboratory.[22] They combined two processes: partial oxidation, which is exothermic, and steam reforming, which is endothermic. Autothermal reforming (ATR) is based on the heat effects of exothermic partial oxidation and endothermic steam reforming and is combined by adding fuel, air and water to the reactor. By controlling the ratio of partial oxidation and steam reforming, the heat balance in the reactor can be controlled. Therefore, external heat supply is not required.[1,2] The general reactions used in this study for different reforming processes combined with autothermal reforming are as follows:

Steam reforming:

$$C_nH_m + 2n\,H_2O \rightarrow n\,CO_2 + \left(\frac{m}{2} + 2n\right) H_2 \quad \Delta H > 0 \qquad (1)$$

$$C_nH_m + n\,H_2O \rightarrow n\,CO + \left(\frac{m}{2} + n\right) H_2 \quad \Delta H > 0 \qquad (2)$$

Partial oxidation:

$$C_nH_m + \left(\frac{n}{2}\right) O_2 \rightarrow n\,CO + \left(\frac{m}{2}\right) H_2 \quad \Delta H < 0 \qquad (3)$$

In ideal case no CO is produced and CO_2 and H_2 are the only products as described by reaction for autothermal reforming:

$$C_nH_m + n\,H_2O + \left(\frac{n}{2}\right) O_2 \rightarrow n\,CO_2 + \left(\frac{m}{2} + n\right) H_2 \quad \Delta H < 0 \qquad (4)$$

In autothermal reforming research, hexadecane is often used as a diesel surrogate. For hexadecane, $n = 16$ and $m = 34$, the enthalpy of reaction is -2053.9 kJ/mol.[2] Hexadecane is a typical hydrocarbon and is well-studied, therefore its chemical and physical data are well known and readily available. The reforming of hexadecane leads to a high yield of H_2. Usually the presence of CO is a problem for proton-exchange membrane (PEM) fuel cells. To solve this problem, a water gas shift reaction (WGS) is used to reduce the content of CO by reacting with water to form CO_2 and H_2.[1,2]

Potential difficulties in autothermal reforming reactors include the occurrence of hot spots and catalyst coking. Compared to autothermal reforming of light hydrocarbons, coking can occur more easily in the reforming of fuels because products such as aromatic compounds and ethylene are precursors of coke.[23] To minimize these difficulties, autothermal reforming reactors must be equipped with a mixing chamber in which the fuel evaporates and mixes with air and steam to form a homogeneous mixture. Complete evaporation of the fuel is critical and can be achieved by some type of atomizer that disperses fuel droplets into a heated zone where the fuel evaporates and mixes with air and steam. Incomplete evaporation can lead to coking if liquid fuel reaches the catalyst. On the other hand, incomplete mixing can lead to local hot spots.[6] Numerous studies have been published on reaction kinetics, mathematical modelling, and optimization of monolithic reactors.[24] Moazami et al.[2] studied a single channel catalytic reactor and developed a numerical two-phase one-dimensional mathematical model. They used a new method for solving conservation equations, such as mass and energy balances, rate equations, and relationships between physical properties. Mentioned method was a combination of Euler's method and the central finite difference method. The advantage is the negligible percentage error caused by the numerical scheme. The influence of thermal conductivity, effective wall thickness of the solid phase and mole fractions of the components was also studied.[2] Zahedi Nezhad et al.[25] published a paper on the autothermal reforming of methane to produce syngas. They proposed a mathematical model for an autothermal reformer consisting of two parts: a combustion part and a catalyst bed part. For the combustion part, they predicted the temperature and composition. For the prediction, they used a mathematical model that included 108 elementary reactions with 28 species. The results from the combustion part served as initial conditions for the catalyst bed part, where they used a one-dimensional heterogeneous reactor model to estimate kinetic parameters and perform kinetic simulations.[25] Gawade et al.[26] studied the reforming and combustion kinetics of n-hexadecane on a rhodium/nickel catalyst supported on alumina. They obtained experimental data in a temperature range of 500°C to 750°C and compared them with three different mechanisms: (a) Eley-Rideal, (b) Langmuir-Hinshelwood bimolecular adsorption and (c) Langmuir-Hinshelwood double site. They also studied combustion kinetics and found that the power-law model provided the best agreement with experimental results.[26] Fazeli and Behnam[27] developed a microreactor and computational fluid dynamics (CFD) model that considered the mechanism of autothermal reforming. The central process in their study was the

autothermal reforming of methane. They used Langmuir-Hinshelwood type kinetic rates. They observed the effects of the type of feed, the ratio of air to fuel, and the addition of water to methane.[27] Malik and Kim[28] published a numerical study on the autothermal reforming of n-hexadecane. They developed a 2D CFD model to study combustion and reforming channels that are thermally coupled and separated by a metal wall. They used rhodium on a CeO_2 support as the catalyst, which was deposited on the inner surface of the channels. Their analysis showed a 86% hydrogen yield with an operating time of 2 h on stream. The operating temperature was between 660 to 850 K. Numerical analysis of autothermal reforming was performed by finite element method using COMSOL as CFD tool. 44 elementary reactions on the catalyst surface were described.[28] Shi et al.[29] developed a numerical model based on CFD, to simulate the performance of a catalytic monolith reactor for hydrogen production. They used an n-hexadecane feed and the reactor was modelled as a porous medium. As a result, they presented the mole fractions for H_2, CO_2 and CO products and temperature changes. They found that the thermal conductivity of the solid catalyst affected the temperature profile in the reactor, but not the hydrogen concentration at the outlet. They found that the reforming efficiency decreased by about 11% when the power input was increased.[29] Liu et al.[30] performed catalytic reforming with dodecane and hexadecane. They investigated a variety of oxygen-carbon and steam-carbon ratios. They found that the oxygen-carbon ratio was most important and strongly influenced the reforming efficiency. The efficiency increased with increasing oxygen-carbon ratio up to 0.42.[30]

Fuel cells powered by hydrogen derived from hydrocarbons can be used as auxiliary power units in vehicles[6] or can power fuel cells in cars.[31,32] Small, compact ATR and WGS reactors are needed for this type of mobile power units. Therefore, an ATR multi-channel reactor (monolith catalyst) of suitable size was considered for an auxiliary power unit and a process was modelled considering both ATR and WGS reactors. The objective of this work is to establish a process model to predict the performance of a proposed integrated autothermal diesel reformer and WGS reactor for hydrogen production. The hydrogen produced in this way is suitable for use in high temperature proton exchange membrane fuel cells (HT-PEMFC), which can be used as auxiliary power units in mobile systems. An initial process model based on thermodynamics is used to determine the influence of process parameters (oxygen-carbon ratio, steam-carbon ratio, influence of temperature at ATR reactor inlet and influence of pressure) on hydrogen yield and CO content after both ATR and WGS reactors. The influence of the parameters on the temperature in the reactors and the cooling power required after the reactors was also investigated. Two surrogates for diesel were considered, one being n-hexadecane and the other a mixture of four different hydrocarbons. Then a kinetic model for the ATR reactor is validated and used to simulate the ATR reactor. In the case of the kinetic model for the WGS reactor, two catalysts, namely FeCr-based and Pt-based, were considered and compared. For the ATR reactor, a catalyst containing cerium oxide, gadolinium oxide and 1 wt% platinum was considered. The kinetic model can be used to predict a system operation and for a design of a real system for hydrogen production from diesel, which would consist of an ATR reactor, a WGS reactor, a sulphur trap and suitable heat exchangers. Thus generated hydrogen would be suitable for auxiliary power units in vehicles.

2 | REACTOR DESIGN AND COMPUTER SIMULATION

2.1 | Reactor design

The main components of the hydrogen production system are the ATR reactor, the sulphur trap and the WGS reactor. The ATR reactor from the work of Liu et al.[30] had a diameter of 38 mm, which is about two times smaller in volume than the one considered here (compact autothermal diesel reformer reactor developed by Fraunhofer IMM[33]), while the length of the reactor was about the same (144 mm). The reactor is designed for conversion of 300 g/h of diesel. Mixing of the reactants takes place in the mixing chamber of the ATR after the mixing nozzle. The inlet is heated with cartridge heaters. For the ideal reactor capacity (300 g/h) 97 W is required to heat the diesel or diesel surrogate mixture. The steam is generated upstream of the ATR with a steam generator that requires 1.4 kW of electrical power. The reactor dimensions considered in this work are as follows:

$$\text{length} = 0.158\,\text{m}$$

$$\text{radius} = 0.0463\,\text{m}$$

$$\text{void fraction} = 0.64.$$

2.2 | Process simulation in Aspen plus

A process diagram was created using ASPEN Plus software to perform Gibbs minimization calculations for the autothermal reforming and water-gas shift reactors (Figure 1). The central parameters were chosen as

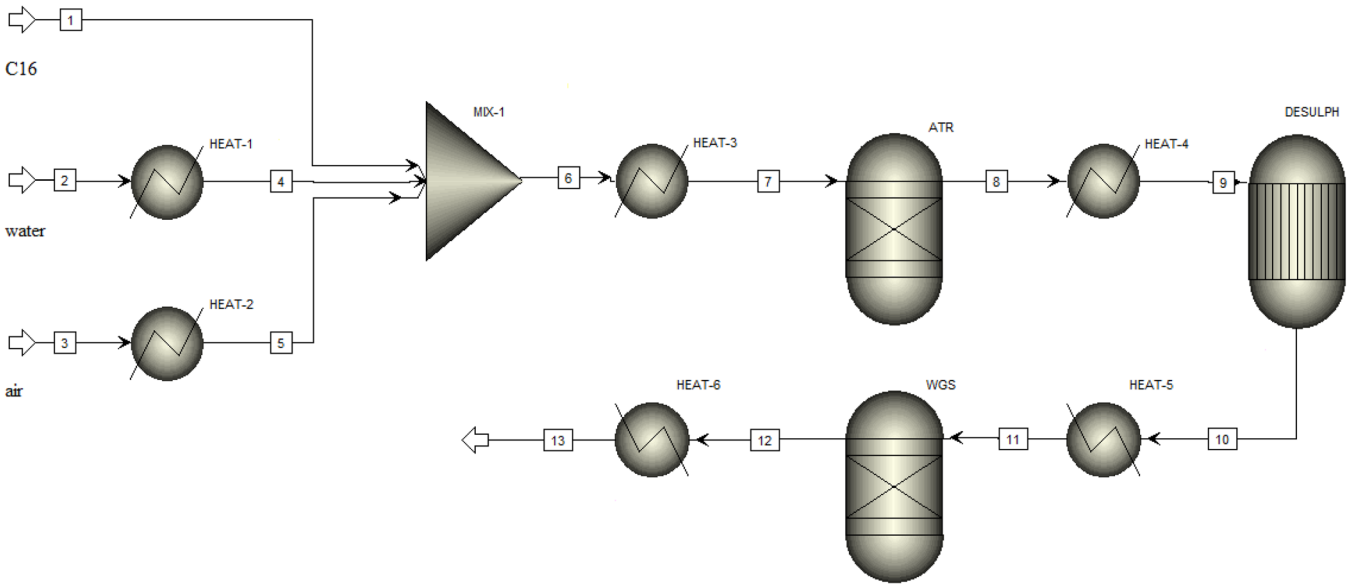

FIGURE 1 The process scheme of the auto-thermal reforming—water-gas shift system.

TABLE 1 Used central parameters

P (bar)	1
O_2 to C ratio	0.475
Steam to C ratio	4
$T_{ATR,in}$ (°C)	400

follows: The feed rate was set at 5 g/min of diesel-surrogate mixture or n-hexadecane as surrogate; a steam-to-carbon ratio of 4 and an O_2/C ratio of 0.475 were used. The temperature at the inlet of the ATR reactor was set at 400°C. The composition of the diesel-surrogate mixture (in mass fractions) was: 0.32 n-hexadecane, 0.42 2,2,4,4,6,8,8-heptamethylnonane, 0.11 trans-decahydronaphthalene, and 0.15 1-methylnaphthalene. The central parameters are listed in Table 1.

The influence of the parameters, namely the ratio of O_2 to C, the ratio of steam to C, and the inlet temperature of the ATR reactor, was studied by varying one parameter while leaving the rest at the central values (Table 1). The ranges of the varied parameters were: O_2 to C ratio from 0.28 to 0.82, steam to C ratio from 2.2 to 6.9, and temperature at the inlet of the ATR reactor from 220°C to 690°C. For the study of the influence of pressure, three cases were considered. In case 1, the original system at 1 bar was used, in case 2, the pressure was 2 bar and the volumetric flow rate was decreased while the molar flow rate remained the same, and in case 3, the pressure was 2 bar and the volumetric flow rate remained the same while the molar flow rate was increased.

2.3 | Kinetic models for ATR and WGS reactors

Both the ATR reactor and the WGS reactor were considered as adiabatic 1D reactors. A 1D plug flow reactor model was used for the mass balance equations of the ATR reactor and a 1D packed bed reactor model was used to describe the WGS reactor. The diesel surrogate was n-hexadecane. Due to the relatively high linear gas velocities, the effect of axial diffusion can be considered insignificant compared to convective flow. Lateral diffusion, on the other hand, could be rate-limiting if too wide channels would be chosen. A full 3D model is needed to investigate this; currently, homogeneous concentration profiles within the channels are assumed. Modelling was performed using Python. The ODE solver's method LSODA was the fastest and most stable for this system of ordinary differential equations. Discretization of the solution was performed for plotting the results on a 201 grid in the x-direction along the channel (in the longitudinal direction).

2.3.1 | ATR reactor kinetic model

The global reaction mechanism for the autothermal n-hexadecane reaction as described in the literature is presented below.[29] The reactions of autothermal reforming are (1) complete combustion, (2 and 4) steam reforming, and (3) water-gas shift reaction. Some n-hexadecane cracking occurs at higher temperatures but is not considered, nor are the balances of the light C1-C4 hydrocarbons, since

their yields are generally low.[29] The reasoning behind complete combustion is that experimental results have shown a higher CO_2 content in the reformer product,[30] in contrast with CO. This mechanism is more accepted in the literature. Based on a previous work,[34] we assumed that CH_4 and other short-chain hydrocarbons are mainly formed by steam or thermal cracking as intermediates rather than methanation. Therefore, CH_4 formation was disregarded because it was assumed that the amount of CH_4 produced is very small. The H_2 deficit due to CH_4 formation was also neglected in the model, which assumes ideal conditions for H_2 formation. Moreover, it has been experimentally demonstrated that the molar fraction of CH_4 in the reformate from autothermal reforming is usually less than 0.5%[30] or not more than 2% in some cases of hexadecane reforming on a different catalyst[35] so the error of the model introduced here due to the exclusion of the methanation reaction is negligible.

Reactions:

1. $2\ C_{16}H_{34} + 49\ O_2 \rightarrow 32\ CO_2 + 34\ H_2O$
2. $C_{16}H_{34} + 16\ H_2O \leftrightarrow 16\ CO + 33\ H_2$
3. $CO + H_2O \leftrightarrow CO_2 + H_2$
4. $C_{16}H_{34} + 32\ H_2O \leftrightarrow 16\ CO_2 + 49\ H_2$

Rate expressions:

$$r_1 = \frac{k_1 P_{C_{16}H_{34}} P_{O_2}^{0.5}}{\left(1 + K_{C_{16}H_{34}} P_{C_{16}H_{34}} + K_{O_2} P_{O_2}^{0.5}\right)^2} \left(\text{kmol } C_{16}H_{34} \text{ reacted}/\text{m}^2\,\text{s}\right)$$

$$r_2 = \frac{k_2 \left(P_{C_{16}H_{34}} - P_{H_2}^3 P_{CO}/P_{H_2O} K_{e2}\right)}{P_{H_2O}^{0.6}} \left(\text{kmol } C_{16}H_{34} \text{ reacted}/\text{m}^2\,\text{s}\right)$$

$$r_3 = k_3 \left(P_{CO} - \frac{P_{H_2} P_{CO_2}}{P_{H_2O} K_{e3}}\right) \qquad \left(\text{kmol CO reacted}/\text{m}^2\,\text{s}\right)$$

$$r_4 = \frac{k_4 \left(P_{C_{16}H_{34}} - P_{H_2}^4 P_{CO_2}/P_{H_2O}^2 K_{e4}\right)}{P_{H_2O}^{0.3}} \left(\text{kmol } C_{16}H_{34} \text{ reacted}/\text{m}^2\,\text{s}\right)$$

$$k_i = A_i\, e^{\left(-\frac{Ea_i}{RT}\right)} \qquad (\text{i} = 1,2,3,4)$$

The partial pressures of the species are in bar, k_i is the reaction rate coefficient, R is the universal gas constant, Ea_i is the activation energy of compound i, $K_{C_{16}H_{34}}$ and K_{O_2} are the absorption equilibrium constants and K_{e_i} are the equilibrium constants and the temperature is T. The reactions take place on the catalyst surface in the monolith with four channels.[29] The surface reaction rates were converted to volume reaction rates by multiplying by the specific surface area of the catalyst ($a_{reactor}$):

$$a_{reactor} = A_{reactor}/V_{reactor}$$

where $A_{reactor}$ is the catalytic surface area (4 × channel cross section × channel length) and $V_{reactor}$ is the channel volume. The value is an approximation and varies with channel dimensions. The reaction rate can be affected by this parameter.

The values for A_i and Ea_i were defined for the catalyst used in the literature data[29,30]: cerium oxide, gadolinium oxide and 1 wt% platinum. In case of other catalytic material, other values can be used.

A 1D plug flow reactor model was used for the mass balance equations. Due to the relatively high linear gas velocities the effect of axial diffusion will be insignificant compared to convective flow. Homogeneous concentration profiles are assumed in the channels. The ordinary differential equations for all species in the system, as well as the heat balance equation are:

$C_{16}H_{34}$:

$$v_x \frac{dc_{C_{16}H_{34}}}{dx} = -r_1 - r_2 - r_4.$$

O_2:

$$v_x \frac{dc_{O_2}}{dx} = -24.5 r_1$$

H_2:

$$v_x \frac{dc_{H_2}}{dx} = 33 r_2 + 49 r_4 + r_3$$

H_2O:

$$v_x \frac{dc_{H_2O}}{dx} = 17 r_1 - 16 r_2 - 32 r_4 - 1 r_3$$

CO:

$$v_x \frac{dc_{CO}}{dx} = 16 r_2 - r_3$$

CO_2:

$$v_x \frac{dc_{CO_2}}{dx} = 16 r_1 + 16 r_4 + r_3$$

Temperature:

$$\rho c_p v_x \frac{dT}{dx} = r_1 \Delta H_1 + r_2 \Delta H_2 + r_3 \Delta H_3 + r_4 \Delta H_4$$

The reaction enthalpies ΔH_1 and ΔH_3 were taken from a paper by Gawade et al.,[26] while $\Delta H_{2,298K}$ was obtained with ASPEN calculations, and $\Delta H_{4,298K}$ was also calculated with ASPEN giving a value of 1820 kJ/mol. The enthalpy of reaction as a function of temperature change was calculated using Kirchhoff's law. The heat capacity of the gas mixture was calculated using the low temperature polynomials NASA a1 to a5 (valid up to 1000 K). The partial pressures and the concentrations are calculated as follows:

$$P_i = c_i \mathrm{RT}$$

The molar fractions through:

$$x_i = \frac{P_i}{\sum P_i}$$

Average density:

$$\rho = \sum P_i M_{\mathrm{avg}}/(\mathrm{RT})$$

2.3.2 | WGS reactor kinetic model

The system of equations is similar to the ATR calculations except that only the WGS reaction occurs in the WGS reactor (reaction 3) and the mass balances are written for the packed bed reactor. The density, heat capacity, enthalpy of reaction, molar mass and partial pressures are treated the same as in the ATR calculations. The mass balances for the packed bed reactor are (ϵ is the void fraction):

H_2:

$$v_x \frac{dc_{H_2}}{dx} = r_{\mathrm{WGS}}(1-\varepsilon)/\varepsilon$$

H_2O:

$$v_x \frac{dc_{H_2O}}{dx} = -r_{\mathrm{RWGS}}(1-\varepsilon)/\varepsilon$$

CO:

$$v_x \frac{dc_{\mathrm{CO}}}{dx} = -r_{\mathrm{RWGS}}(1-\varepsilon)/\varepsilon$$

CO_2:

$$v_x \frac{dc_{CO_2}}{dx} = r_{\mathrm{RWGS}}(1-\varepsilon)/\varepsilon$$

For the calculations, the inlet conditions were assumed for the case that the ATR reactor is operated with the central parameters:

$$T_{C_{\mathrm{in}}} = 300\,^{\circ}\mathrm{C}\,(\mathrm{WGS\,temperature})$$

Flow rate:

$$\phi_{\mathrm{vol,in}} = 0.0021216\,\mathrm{m}^3/\mathrm{s}$$

Inlet components (%):

$$x_{C_{16}H_{34},0} = 0$$

$$x_{O_2,0} = 0$$

$$x_{H_2,0} = 22.2634$$

$$x_{H_2O,0} = 41.3159$$

$$x_{\mathrm{CO},0} = 4.2671$$

$$x_{CO_2,0} = 8.2918$$

$$x_{N_2,0} = 23.8619$$

The dimensions of the reactor are as follows; a typical void fraction for a packed bed was assumed:

$$\mathrm{length} = 0.144\,\mathrm{m}$$

$$\mathrm{width} = 0.054\,\mathrm{m}$$

$$\mathrm{depth} = 0.086\,\mathrm{m}$$

$$\text{void fraction}\,(\varepsilon) = 0.4$$

A typical bulk catalyst density was also presumed:

$$\rho_{\mathrm{cat}} = 1000\,\mathrm{kg/m}^3$$

The thermodynamic equilibrium for WGS is (T in K):

$$K_{\mathrm{eq}} = 10(-2.4198 + 0.0003855\,T + 2180.6/T)$$

For the solution, the same methodology and solver (LSODA) as in the case of and ATR reactor were used to solve the set of ODEs.

Two cases of the kinetic model were considered. In the first case kinetic parameters for the FeCr-based

catalyst[36] and in the second case, kinetic parameters for the Pt-based catalyst were used.[37]

Kinetic parameters for reaction rate in the form of power law for FeCr-based catalyst are[36]:

$$n_{CO}\,(a) = 1$$

$$n_{H_2O}\,(b) = 0$$

$$n_{CO_2}\,(c) = -0.36$$

$$n_{H_2}\,(d) = -0.09$$

$$A_{WGS} = 700 \times 10^3\ \text{mol/kg s kPa}^{-n_{CO}-n_{H_2O}-n_{CO_2}-n_{H_2}}$$

$$Ea_{WGS} = 110 \times 10^3\ \text{J/mol}$$

$$R_{WGS} = kP_a^{CO}P_b^{H_2O}P_c^{CO_2}P_d^{H_2}(1-\beta)$$

Where partial pressures are in kPa.

The kinetic expression for the Pt-based catalyst ($Pt/CeO_2/Al_2O_3$) is in the Langmuir-Hinshelwood form[37]:

$$K_{CO} = 94.4$$

$$K_{H_2O} = 12.2$$

$$K_{H_2} = 462$$

$$K_{CO_2} = 2.4$$

$$A_{WGS} = 3.7 \times 10^7 \frac{\text{mol}}{\text{kg}\,s}$$

$$Ea_{WGS} = 78.2 \times 10^3\ \text{J/mol}$$

$$r_{CO} = \frac{k_{rds}K_{CO}K_{H_2O}P_{CO}P_{H_2O}(1-\beta)}{\left(1+K_{CO}P_{CO}+\sqrt{K_{H_2}P_{H_2}}\right)^2\left(1+\sqrt{K_{H_2O}P_{H_2O}}+K_{CO_2}P_{CO_2}\right)}$$

$$\beta = \frac{1}{K}\frac{P_{CO_2}P_{H_2}}{P_{CO}P_{H_2O}}$$

3 | RESULTS

3.1 | Aspen model and influence of parameters

Figure 2 shows the Gibbs minimization results for the diesel-surrogate mixture, and Figure S1 in the supporting information shows the process schematic with Gibbs minimization results for the n-hexadecane surrogate. For the simulation in the second case, 5 g/min of n-hexadecane was used, yielding 1.325 mol/h. 84.8 mol/h of water and 50.35 mol/h of air are used, giving an O_2 to C ratio of 0.475 and an S to C ratio of 4. Heating the air to 400°C requires 0.157 kW of power, heating the n-hexadecane requires 0.13 kW, and heating the water stream requires 1.411 kW. All feed streams are heated to 400°C before entering the ATR reactor. The outlet temperature of the ATR reactor is raised to 739°C due to the exothermic reaction and 0.7 kW is required to remove the heat and reach 310°C for the desulfurizer. In the WGS reactor, the reaction is also exothermic and the temperature is raised from 300°C at the inlet to 338°C.

The Gibbs minimization solution for the surrogate mixture (Figure 2) gives a slightly higher ATR outlet temperature (766°C) and a slightly higher WGS outlet temperature (340°C), otherwise the solutions are very similar to the case with n-hexadecane. The molar fraction at the outlet of CO before condensation (stream 12) is 0.35%, while this value can be reduced to 0.20% if the WGS reactor is operated in isothermal mode, which keeps the outlet temperature at 300°C and favours thermodynamic equilibrium with less CO. The molar fraction of CO at the outlet after the condensation (stream 13) would be 0.34%. By Gibbs minimization, the equilibrium concentrations at different temperatures can be obtained. In order to calculate the required capacities for the equipment design, kinetic mechanisms, rate expressions, and kinetic data coupled with the governing transport phenomena through appropriate heat and mass balances for the specific reactor design are required. This will be investigated in the following sections. First, the influence of the process parameters in the process model is examined and then the kinetics in the two reactors are considered.

3.1.1 | Influence of O_2 to C ratio

Figure 3 shows the gas composition at the outlet of the ATR (Figure 3A) and WGS (Figure 3B) reactors at different oxygen to carbon ratios. Here, air is used as the oxygen source, as this would be most practical in a real system. As can be seen in all the cases presented, the diesel surrogate mixture and oxygen are completely depleted. Most importantly, the amount of hydrogen produced decreases rapidly as more oxygen reacts with C16 (yellow curve in Figure 3A,B). If the H_2 molar fraction at the ATR output is about 0.22 at the central conditions of 0.475 O_2/C ratio, it decreases to only 0.1 at 0.8 O_2/C ratio. On the other hand, more hydrogen is produced when the

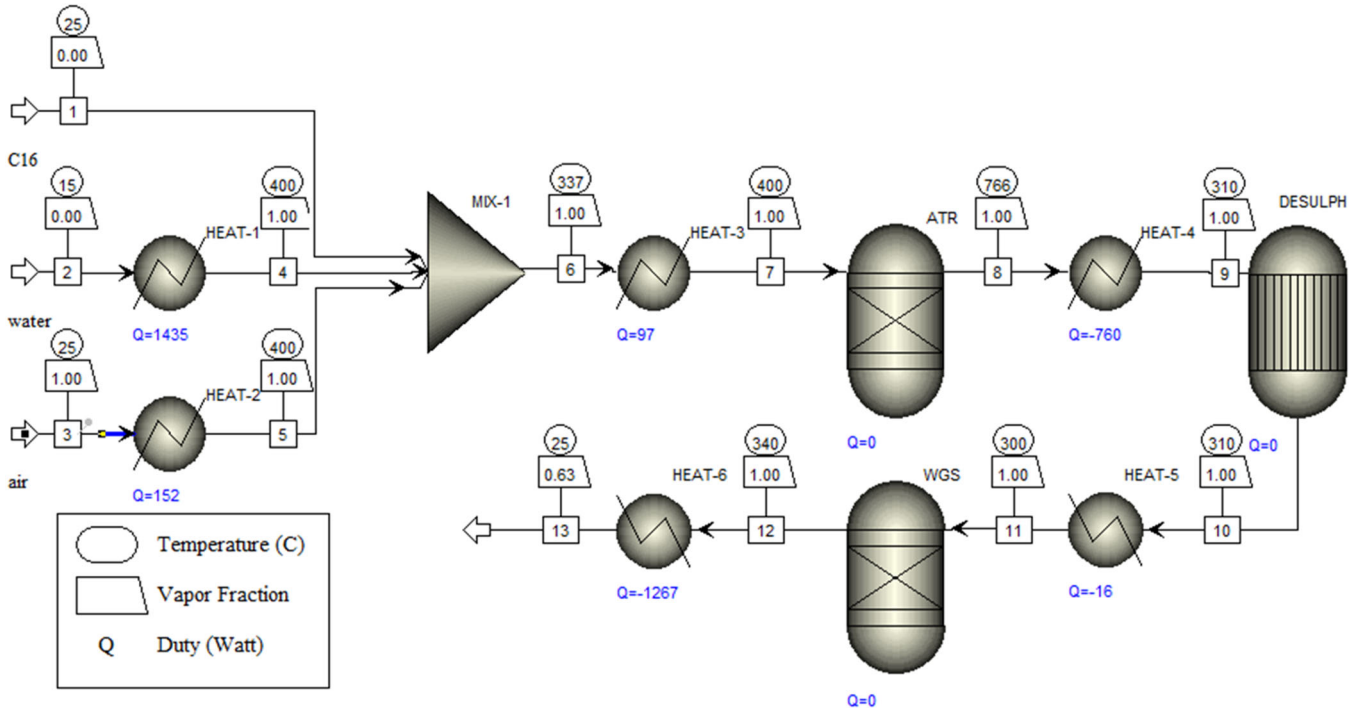

FIGURE 2 The ASPEN Plus process diagram of the autothermal reforming and water-gas shift reactor system for a diesel surrogate mixture

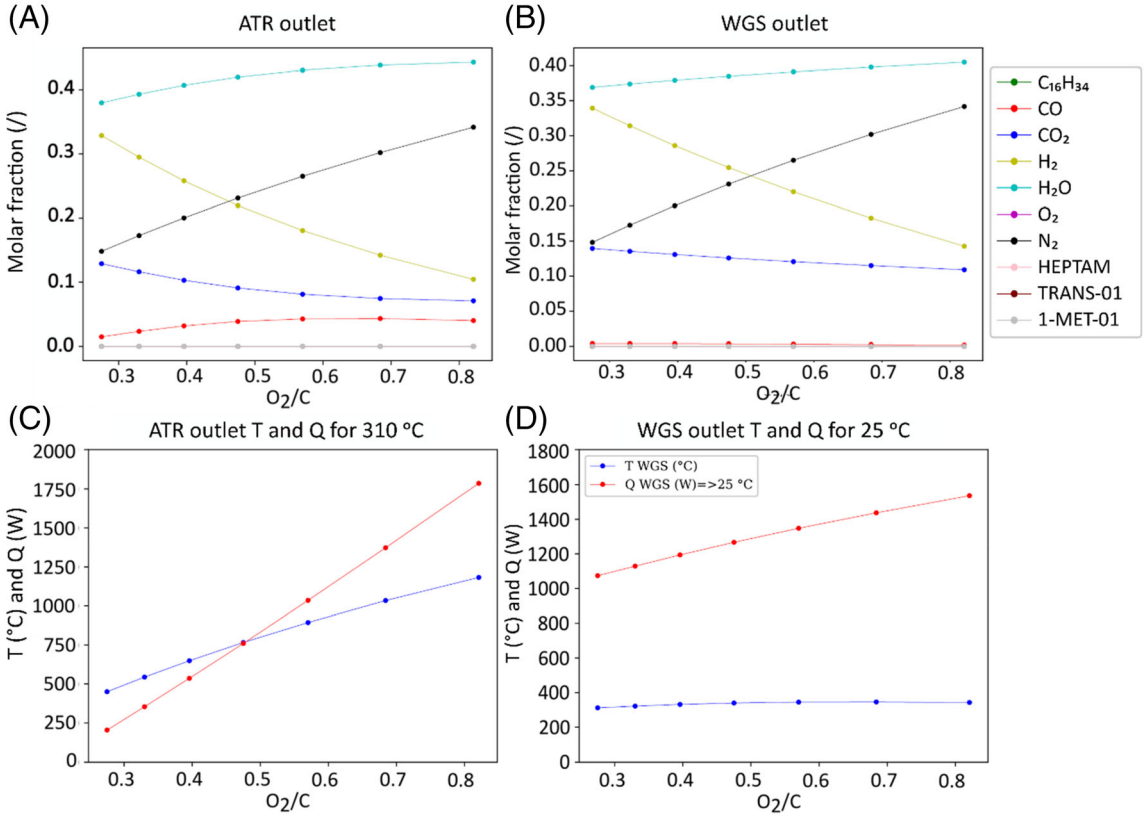

FIGURE 3 Results at different oxygen-carbon ratios. (A) auto-thermal reforming (ATR) reactor outlet gas composition, (B) water-gas shift (WGS) reactor outlet gas composition, (C) ATR outlet temperature and the power required to subsequently reduce it to 310°C, (D) WGS outlet temperature and the power required to reduce it to 25°C

amount of O_2 is decreased; at an O_2/C ratio of 0.3, the molar fraction of H_2 is more than 0.3. It is obvious that the H_2/CO ratio is also worse at a higher O_2/C ratio than when less oxygen is present. At the lowest O_2/C ratio, the molar fraction of H_2 is 23 times greater than the molar fraction of CO. At the highest O_2/C ratio, the ratio of H_2 to CO is only 2.6. The content of CO can be significantly reduced by the WGS reaction. As can be seen in Figure 3B, the gas composition at the exit of the WGS reactor is similar to that at the ATR outlet except for the effect of the water-gas shift that occurred. We can see that CO drops to a very small amount at all O_2/C ratios, less water, more CO_2, and also more H_2 are produced (Figure 3B). The H_2 content increases from 0.329 at the outlet of the ATR reactor to 0.340 at the outlet of the WGS reactor for the lowest O_2/C ratio and from 0.104 before the WGS reactor to 0.143 after the WGS for the highest O_2/C ratio. Oxygen is needed for autothermal operation. Thus, a decrease in O_2 content has a negative effect as the temperature in the ATR decreases and the reaction slows down and eventually stops altogether. Figure 3C shows the ATR outlet temperature and the power required to reduce the temperature to 310°C. At the highest O_2/C ratio, the exit temperature reaches 1182°C. It should be noted that the maximum temperature inside the ATR is much higher due to the exothermic reaction with O_2. The final temperature is reached after the endothermic reaction of the remaining C16 with water. As mentioned earlier, the heat release of the water has a great influence on the system. The temperature at the outlet of the adiabatic WGS reactor increases slightly from 312°C at the lowest O_2/C ratio to 343°C at the highest value because the gas entering the WGS reactor is farther from equilibrium conditions and consequently a larger increase in conversion occurs. This, and the fact that there is more water in the system, means that much more energy is needed to cool the gas to room temperature: 1.54 kW compared to the 1.27 kW at the central conditions, as shown in Figure 3D.

3.1.2 | Influence of steam to carbon (S/C) ratio

In general, the amount of H_2 that can be produced in the ATR is determined by the residue of C16 after reaction with O_2. Additional hydrogen can be produced by a water gas shift reaction. More water in the feed can have a negative effect because it increases the required heating power. However, it should be noted that water plays an important role in preventing excessive coking.[23] Figure 4 shows the different results at different S/C ratios. From the results in Figure 4A another positive effect is a decrease in the concentration of CO due to the water gas shift reaction; the higher amount of water shifts the thermodynamic equilibrium, causing CO to decrease and CO_2 to be formed. At higher S/C, more CO_2 is produced, but since the amount of water also increases, the molar fraction is about the same. While the water content in the ATR reactor increases, the molar fraction of H_2 decreases. However, comparison with the molar fraction of CO shows that increasing the S/C ratio improves the H_2/CO ratio. At the lowest S/C value, about 3.1 times more H_2 is produced than CO. At the highest S/C value, the ratio of H_2 to CO is about 12. Therefore, by increasing the S/C ratio, a purer hydrogen can be obtained in terms of the CO content. The same conclusions can be drawn for the WGS reactor as for the O_2/C ratio: CO and H_2O react to form CO_2 and H_2 (Figure 4B). Figure 4C shows the ATR outlet temperature and the power required to cool it to 310°C. Excess water in the ATR means that the energy released by the C16 and O_2 reactions is used to heat water, decreasing the outlet temperature (from about 850°C at the lowest S/C ratio to about 680°C at the highest ratio). Interestingly, a lower outlet temperature does not result in a lower required cooling power; in fact, it is higher at lower temperatures due to the higher water content. The very high increase in cooling power after the WGS reactor in Figure 4D is again a consequence of the high water content. At the lowest S/C ratio, the mass flow of water is 0.9 kg/h, while at the highest it is 2.7 kg/h, which is a threefold increase.

3.1.3 | Influence of inlet ATR temperature

The effect of ATR input temperature can also provide insight into how the integrated system responds to the desired or potentially undesired change in operation.

Figure 5A, clearly shows that the difference between the molar fractions corresponds exactly to the change in the water-gas shift equilibrium from temperature 630°C to 1000°C (seen in Figure 5C). At a higher outlet temperature, there is a higher water and CO content and a comparatively lower H_2 and CO_2 content. At an inlet temperature of less than 400°C, achieving complete conversion would require a very long residence time. At the lowest ATR inlet temperature for which the calculation was performed, the H_2/CO ratio is 9. At the highest temperature, it drops to only 3.6. However, the additional WGS reactor can decrease the CO content and the H_2/CO ratio is increased to about 90 for all ATR inlet temperatures. At the output of the WGS reactor, no effect of the ATR input temperature is observed because the gas composition is converted to the equilibrium composition at the WGS reactor temperature in all cases, as shown in

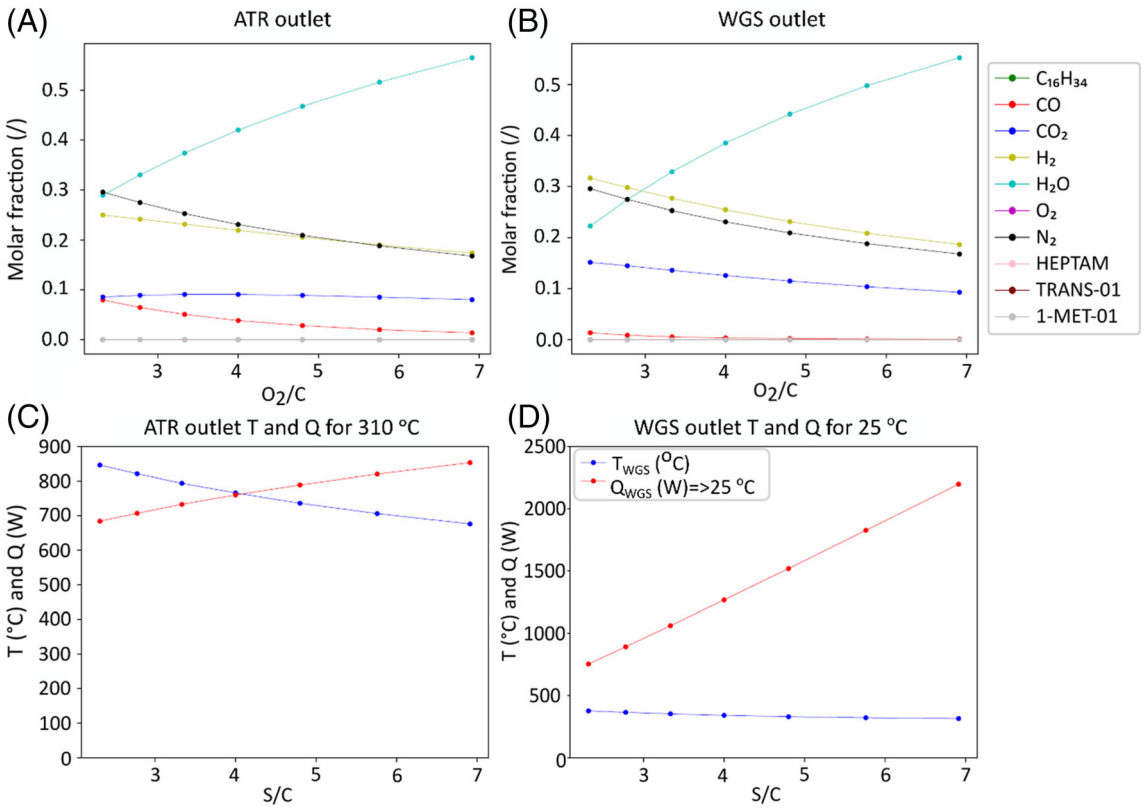

FIGURE 4 Results at different ratios of steam to carbon. (A) Gas properties at the outlet of the auto-thermal reforming (ATR) reactor, (B) Gas properties at the outlet of the water-gas shift (WGS) reactor, (C) ATR outlet temperature and power required for cooling to 310°C (D) WGS outlet temperature and power required for cooling to 25°C

Figure 5B. However, there are differences. The inlet gas composition is different; at higher temperatures it shifts to CO and H_2O. This means that at the lower WGS temperatures, a higher conversion is required to reach equilibrium, causing a larger temperature rise due to the exothermic WGS reaction. In the considered range, the WGS exit temperature is between 326°C and 359°C (Figure 5D). This can be observed at CO where the molar fraction is increased from about 0.0029 to 0.0043.

3.1.4 | Influence of pressure

The same central parameters were considered. The ratio of O_2 to C was 0.475 and the ratio of S to C was 4. The resulting gas composition is shown in Table S1 and the results of all three cases are identical. This is correct because the gas composition at the outlet depends only on the composition of the diesel surrogate and the $C/O_2/H_2O$ ratio (since ATR reactions are irreversible) and the temperature of the WGS reactor. Also the pressure has no influence on the operation of the WGS reactor, since the reaction is equimolar.

3.2 | ATR reactor kinetic model

The model was compared with the available experimental results from Reference [29]. The temperature at the inlet was 327°C, the pressure was 2 bar, the flow rate of n-hexadecane was 2.0445 mol/h, the flow rate of water was 65.408 mol/h, the flow rate of air was 60.5 mol/h. The reactor length was 143.92 mm, the radius of the reactor tube was 19.05 mm, and the void fraction was 0.64, resulting in the following residence times (τ), ratio of O_2 to C (O_2/C ratio), and ratio of steam to C (S/C ratio): $\tau = 0.12$ s, O_2/C ratio = 0.370 and S/C ratio = 2.000.

The temperature profile in this case is in good agreement with the experiments (Figure 6A). The experimental outlet temperature is 690°C, while the simulated value is 737°C, which could be due to heat loss to the environment. The initial oxidation rate is extremely high. Heat is released, which further increases the reaction rate until the O_2 is depleted. Then the endothermic steam reforming reaction begins to decrease the temperature. The molar concentrations of all components are shown in Figure S2 in the supporting information. The profiles are different as the number of moles increases during the

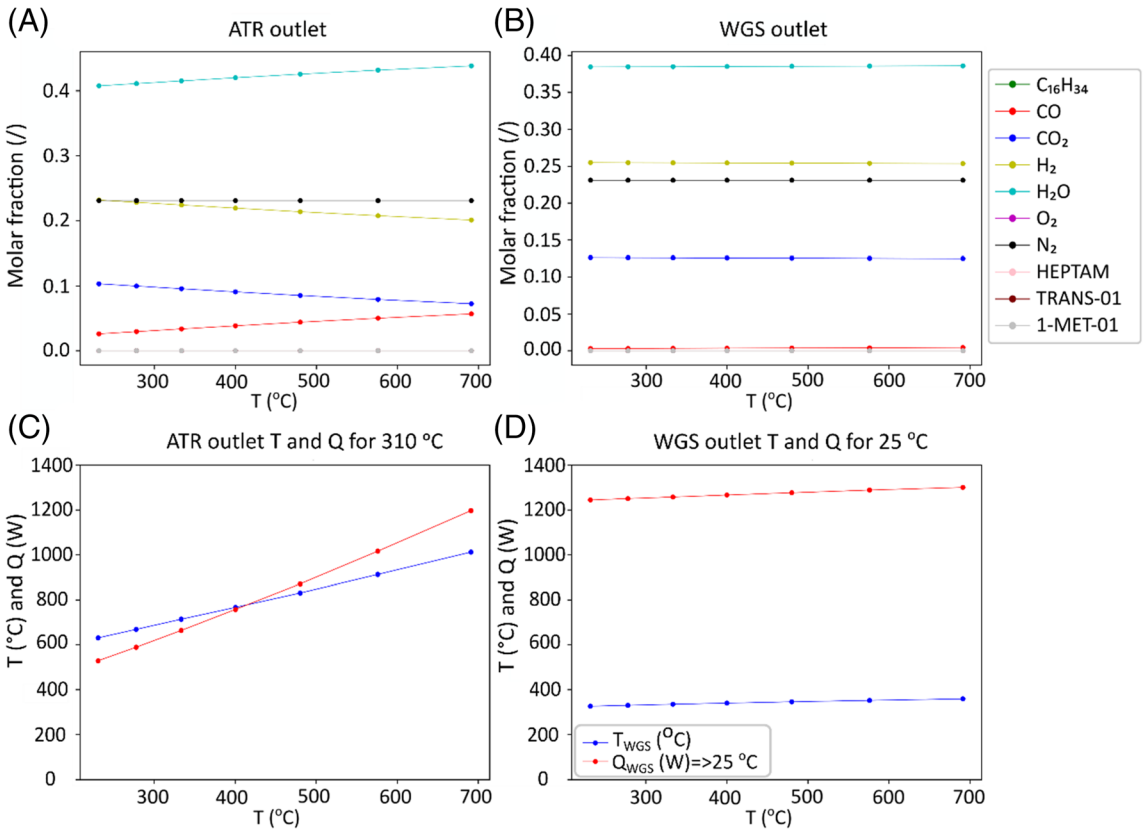

FIGURE 5 Results at different inlet temperatures (in°C). (A) Gas composition at auto-thermal reforming (ATR) reactor outlet, (B) Gas composition at water-gas shift (WGS) reactor outlet, (C) ATR outlet temperature and power required for cooling to 310°C (D) WGS outlet temperature and power required for cooling to 25°C

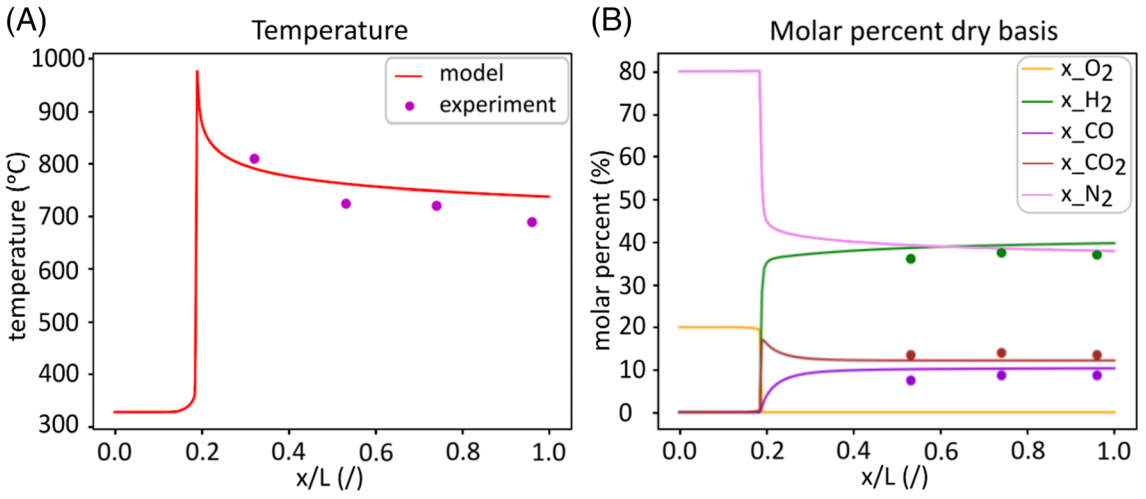

FIGURE 6 Temperature profiles calculated with the model compared to experimental data[29] (A) and the molar fraction of dry components in the gaseous mixture compared to experimental data[29] (B)

reactions. The final gas composition depends on the initial reactant ratios (steam and O_2 to C) and the final temperature due to the equilibrium of the water-gas shift reaction.

The simple 1D model for the ATR reactor showed a good agreement with the experimental results from Reference [29] and can therefore be used to model a different reactor design, keeping the same reaction rate

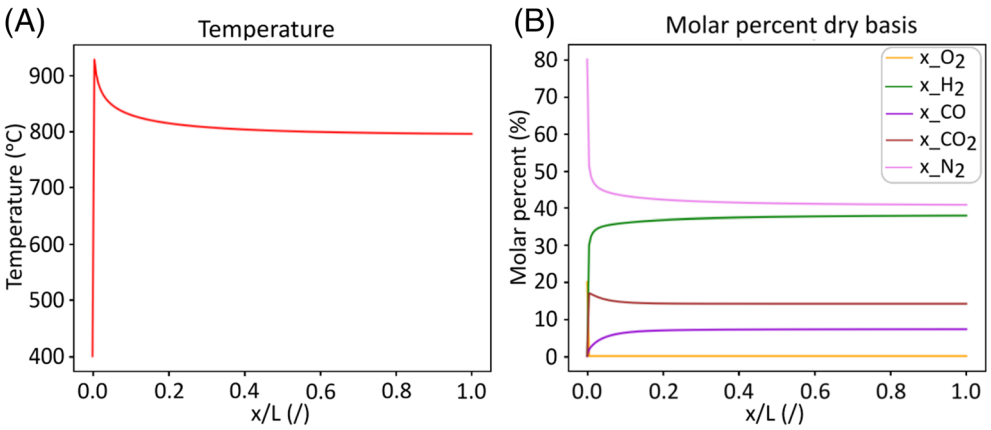

FIGURE 7 The temperature profile and mole percent profiles (dry basis) inside the auto-thermal reforming reactor

expressions and kinetic parameters if the same monolith catalyst is used. The following operating parameters were used based on the ATR reactor design considered herein with an optimum capacity of 300 g/h of diesel surrogate. The void fraction for the catalyst was taken from Reference [29] and had a value of 0.64. Inlet temperature:

$$T_{C,in} = 400\ ^{\circ}\mathrm{C}$$

Flow rates:

$$F_{C_{16}H_{34},0} = 1.325 \frac{\mathrm{mol}}{\mathrm{h}};$$

$$F_{H_2O,0} = 84.8 \frac{\mathrm{mol}}{\mathrm{h}};$$

$$F_{\mathrm{air},0} = 50.35 \frac{\mathrm{mol}}{\mathrm{h}}$$

The oxygen to carbon and water to carbon values were the same as in Table 1. The reactor was approximated using a cylindrical shape with a length of 158 mm and a radius of 46.3 mm. Figure 7A shows the temperature profile. An outlet temperature of about 800°C is obtained. This is the same value obtained from the manual calculation, as opposed to the value of 750°C obtained with Gibbs minimization. In any case, the calculations are close enough to give a rough idea of what to expect in the reactor. Figure 7B shows the mole percentages on a dry basis along the length of the reactor. The temperature at the reactor inlet is immediately raised to about 930°C by rapid exothermic partial oxidation. Shortly after the reactor inlet, oxygen is rapidly consumed (Figure 7B) and the temperature drops due to the endothermic steam reforming reaction. The temperature stabilizes about midway through the reactor. 100% conversion of O_2 and n/hexadecane is achieved at the chosen conditions. This is presented in Figure S3 in Supporting information where concentration profiles of all the compounds in the reactor are shown. Both hexadecane and oxygen are consumed immediately after the reactor inlet. 38% of the hydrogen on a dry basis can be obtained in this way when air is used as the oxygen source. The carbon monoxide content that can be reduced with the WGS reactor is 7%. As a two times higher ratio of steam to carbon is used here than in reference [24] and because of the high heat capacity of water, the temperature profile is somewhat flattened compared to the profile in Figure 6. The temperature profile in Figure 7 has a lower maximum temperature and a less steep drop.

3.2.1 | Influence of pressure

The kinetic expressions are complex and nonlinear, so it is difficult to predict the effects of increased pressure, but the model solutions suggest that the overall reaction rate decreases at higher pressure. The residence time for the first case was reduced to achieve approximately 80% conversion at the reactor outlet. Three scenarios were compared:

Case 1. Original system at 1 bar. Vol. flow rate = 7.63 m^3/h, mol. Flow rate = 136.44 mol/h

Case 2. Pressure = 2 bar; volumetric flow decreased to 3,82 m3/h; molar flow is the same.

Case 3. Pressure = 2 bar; volumetric flow is the same; molar flow increased to 272.9 mol/h.

The conversions in all three cases are shown in Figure 8. In case 2, where the volumetric flow rate decreases, the residence time is subsequently increased by a factor of 2, resulting in a higher conversion (86.5%), while case 3 has the same residence time and consequently a lower conversion than the original 1 bar case (81.55%).

The following conclusions can be derived:

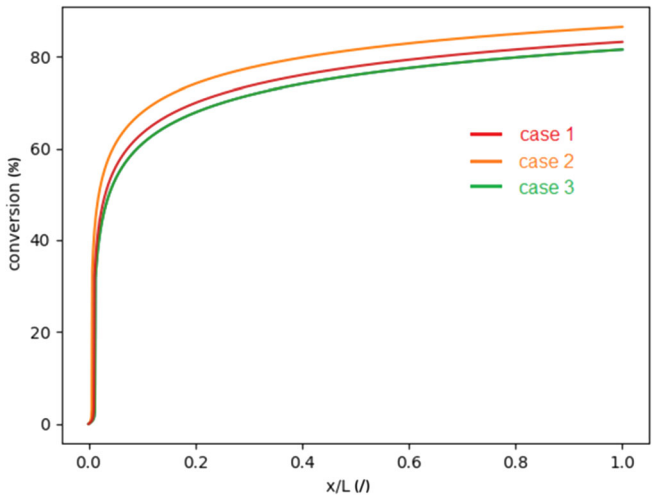

FIGURE 8 C16 conversions along the length of the ATR

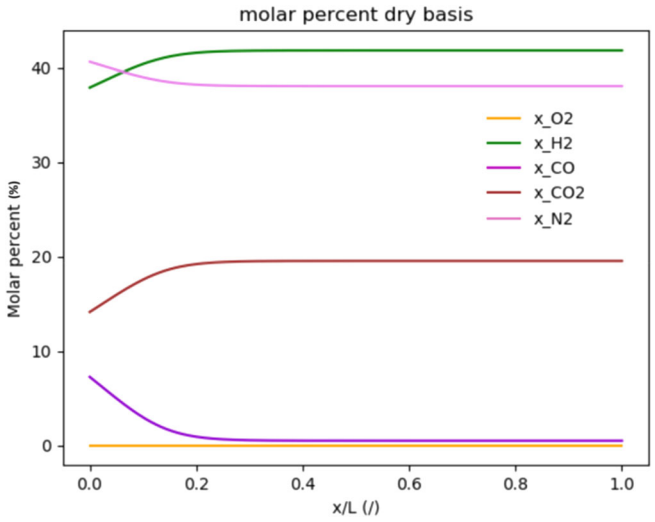

FIGURE 9 The molar percentage on dry basis profile in water-gas shift reactor at 300°C inlet temperature and Pt-based catalyst

- The composition of the exhaust gas under equilibrium conditions is independent of the pressure of the system.
- If the pressure is increased to 2 bar with an exhaust valve or a backpressure regulator, the volumetric flow rate decreases by a factor of 2, while the molar flow rate remains the same (case 2).
- If the volumetric flow rate is increased to increase the molar flow rates, the energy requirement also increases by a factor of 2 (case 3). A larger amount of hydrogen is produced for the fuel cell.
- Compared to the original case at 1 bar, case 2 results in a higher conversion due to the longer residence time, while case 3 results in a lower conversion due to the slower kinetics at the increased pressure.
- Operation at the increased pressure of 2 bar should not be problematic as the pressure has no effect on the exhaust gas, while the possible reduction in conversion, if problematic, could be solved by using a larger reactor volume or a larger amount of catalyst.

3.3 | WGS reactor kinetic model

The WGS reaction is kinetically favoured at higher temperatures, but thermodynamic equilibrium favours less CO formation at lower temperatures. Since the fuel cell can be operated at a CO content of less than 1%, the temperature of 300°C should be appropriate to achieve a fast reaction to low CO concentrations. Low temperature shift (LTS) copper-based catalysts tend to sinter at temperatures above 250°C, so a high temperature shift catalyst (HTS) would be more appropriate.

The results of the model for the WGS reactor in the case with FeCr-based catalyst are shown in Figure S4 (temperature profile) and in Figure S5 (mole percent of compounds on dry basis) in the supporting information. For the case with Pt-based catalyst, the results are shown in Figure S5 (temperature profile) and in Figure S6 (mole percent of compounds on dry basis) in the supporting information. In the case of the FeCr-based catalyst, the reaction did not occur at 300°C. A temperature of 450°C was required (Figure S3). Figure S4 shows the decrease in CO and H_2O, but a significant amount of CO is still present. At this temperature (before condensation), more than 1% of CO remains in the exhaust gas. After condensation, this value is higher. The conclusion is that FeCr-based catalysts are not suitable to reach the required capacities. The required temperature is too high and too much CO is produced. A downstream WGS reactor with low temperature would be required.

The $Pt/CeO_2/Al_2O_3$ was much more active and the equilibrium conversion was achieved at an inlet temperature of 300°C. The calculated exit temperature was 328°C (Figure S6 in the supporting information). Figure 9 shows a much larger decrease in CO concentration at these temperatures. 270 g of catalyst was positioned in the reactor and equilibrium was reached after about 30% of the length of the packed bed reactor. The CO concentration decreased to 0.6%, which is much more suitable for fuel cells than the CO content obtained with an FeCr-based catalyst.

3.4 | Comparison of the kinetic models with ASPEN

The composition at the reactor outlet corresponds to the values obtained by Gibbs minimization, seen in detail in

TABLE 2 Comparison of composition obtained with auto-thermal reforming (ATR) kinetic model and with ASPEN Gibbs minimization with n-hexadecane as diesel surrogate and water-gas shift (WGS) (Pt-Based catalyst) kinetic model compared to ASPEN Gibbs minimization

Component	Molar fraction (%) 1D kinetic model ATR out	Molar fraction (%) Gibbs minimization ATR out	Molar fraction (%) 1D kinetic model WGS out	Molar fraction (%) Gibbs minimization WGS out
$C_{16}H_{34}$	0	0	0	0
O_2	0	0	0	0
H_2	22.26	22.88	26.21	25.07
H_2O	41.32	40.70	37.37	37.57
CO	4.27	3.65	0.320	0.334
CO_2	8.29	8.9	12.24	12.04
N_2	23.86	23.86	23.86	24.98

Table 2. The gas composition in the case of the ATR reactor is accurate to less than 1%. The small difference between the kinetic and thermodynamic models is due to the fact that the temperature calculated by the kinetic model is about 50°C higher, resulting in a higher CO equilibrium concentration. In the case of the WGS reactor, both models give almost the same results, which confirms that the kinetic model for the WGS reactor was also accurate and can be used for further development. Different operating scenarios and other catalysts can be tested, as well as the sensitivity of the system to variations in operating parameters, which is useful when deviations from ideal operation occur. Reaction rates can be modified by the operating temperature of the ATR, which can be varied with the O_2 inlet content.

4 | CONCLUSIONS

A computational study of the ATR-WGS system for hydrogen production from diesel for fuel cell applications in mobile units was performed. For high temperature PEM fuel cells, the lowest possible CO content in the generated hydrogen is desirable. First, the influence of the parameters in Aspen was studied, then kinetic models were used to model the concentration and temperature profiles of the two reactors ATR and WGS. The results of the Aspen model with the diesel-surrogate mixture show that more hydrogen is produced at a low O_2/C ratio than at a higher ratio. Most important is the effect of this ratio on the temperature in the ATR reactor. When the O_2/C ratio is too low, the temperature in the ATR reactor decreases because not enough heat is released by partial oxidation. At the lowest O_2/C ratio (0.28), the temperature is 450°C and at a ratio of 0.8 it approaches 1200°C. Increasing the ratio of steam to carbon decreases the CO content at the outlet of the ATR reactor because more steam is available for the water gas shift reaction. If the H_2O/C ratio is sufficiently high, the CO content at the outlet of the WGS reactor can be reduced to as low as 0.15 mol% when considering the entire product mixture. At a high H_2O/C ratio, a lower temperature at the outlet of the ATR reactor can be achieved, but the cooling power to reach the inlet temperature of the WGS reactor must be greater than at a low H_2O/C ratio because of the high water content. In all cases considered, the WGS reactor reduces the molar fraction of CO below 0.02. The kinetic model for the ATR reactor design considered shows that a large temperature rise can be expected at the reactor inlet due to the rapid and exothermic partial oxidation of n-hexadecane (diesel surrogate used for the kinetic model). The temperature will reach about 930°C in a fraction of the reactor length before oxygen is completely consumed, and will decrease along the length of the reactor to reach almost 800°C at the outlet. This reactor yields 38 mol% hydrogen on a dry basis. Kinetic models for the WGS reactor show that a Pt-based catalyst is more suitable than an FeCr-based catalyst because a lower temperature is required for a Pt-based catalyst to reach a lower CO content. Equilibrium is reached within one-third of the reactor length. It was shown that simple kinetic models for both the ATR reactor with monolithic catalyst and the WGS fixed-bed reactor are suitable for simulating the behaviour of autothermal reforming of diesel and can be used to predict and control the operation of the reactor in a real system. Future work includes the construction of an experimental setup using the ATR reactor design considered here with a suitable desulfurization system and a WGS reactor. The kinetic models will then be validated and, if needed, adapted to the actual diesel feedstock and used to control and/or intensify the process.

ACKNOWLEDGMENTS

The authors acknowledge Slovenian Research Agency for funding through the research project J2-1724 and

research core funding P2-0152. The work was also supported by the Development of an Innovative Auxiliary Power UNIT based on high-temperature PEM fuel cell and reforming technology for logistic fuels (IAPUNIT) research project co-funded by European Defence Agency (B 1490 GEM 3 GP) and Slovenian Ministry of Defence. Dr. Andrej Pohar is gratefully acknowledged for providing valuable guidelines during the preparation of the manuscript.

DATA AVAILABILITY STATEMENT

Data openly available in a public repository that issues datasets with DOIs

ORCID

Dimitrij Ješić https://orcid.org/0000-0002-4628-4104
Blaž Likozar https://orcid.org/0000-0001-7226-4302

REFERENCES

1. Kang I, Bae J. Autothermal reforming study of diesel for fuel cell application. *J. Power Sources.* 2006;159:1283-1290. doi:10.1016/j.jpowsour.2005.12.048
2. Moazami N, Wyszynski ML, Mahmoudi H. Modeling of catalytic monolith reactor for reforming of hexadecane with exhaust gas. *Int. J. Hydrogen Energy.* 2013;38:11826-11839. doi:10.1016/j.ijhydene.2013.06.122
3. Zazhigalov SV, Rogozhnikov VN, Snytnikov PV, et al. Simulation of diesel autothermal reforming over Rh/-Ce0.75Zr0.25O2-δ-η-Al2O3/FeCrAl wire mesh honeycomb catalytic module. *Chem. Eng. Process. - Process Intensif.* 2020;150:107876. doi:10.1016/j.cep.2020.107876
4. Kang I, Bae J, Bae G. Performance comparison of autothermal reforming for liquid hydrocarbons, gasoline and diesel for fuel cell applications. *J. Power Sources.* 2006;163:538-546. doi:10.1016/j.jpowsour.2006.09.035
5. Samsun RC, Prawitz M, Tschauder A, Pasel J, Peters R, Stolten D. An autothermal reforming system for diesel and jet fuel with quick start-up capability. *Int. J. Hydrogen Energy.* 2019;44:27749-27764. doi:10.1016/j.ijhydene.2019.08.244
6. Xu X, Li P, Shen Y. Small-scale reforming of diesel and jet fuels to make hydrogen and syngas for fuel cells: a review. *Appl. Energy.* 2013;108:202-217. doi:10.1016/j.apenergy.2013.03.028
7. Bae M, Cheon H, Oh J, Kim D, Bae J, Katikaneni SP. Rapid start-up strategy of 1 kWe diesel reformer by solid oxide fuel cell integration. *Int. J. Hydrogen Energy.* 2021;46:26575-26581. doi:10.1016/j.ijhydene.2021.05.115
8. Song Y, Han K, Wang D. Thermodynamic analysis of fossil fuels reforming for fuel cell application. *Int. J. Hydrogen Energy.* 2020;45:20232-20239. doi:10.1016/j.ijhydene.2019.11.175
9. Malik FR, Tieqing Z, Kim Y-B. Temperature and hydrogen flow rate controls of diesel autothermal reformer for 3.6 kW PEM fuel cell system with autoignition delay time analysis. *Int. J. Hydrogen Energy.* 2020;45:29345-29355. doi:10.1016/j.ijhydene.2020.07.208
10. Fan MS, Abdullah AZ, Bhatia S. Catalytic technology for carbon dioxide reforming of methane to synthesis gas. *ChemCatChem.* 2009;1:192-208. doi:10.1002/cctc.200900025
11. Wang S, Lu GQ, Millar GJ. Carbon dioxide reforming of methane to produce synthesis gas over metal-supported catalysts: state of the art. *Energy Fuels.* 1996;10:896-904. doi:10.1021/ef950227t
12. Zhang G, Liu J, Xu Y, Sun Y. A review of CH4-CO2 reforming to synthesis gas over Ni-based catalysts in recent years (2010-2017). *Int. J. Hydrogen Energy.* 2018;43:15030-15054. doi:10.1016/j.ijhydene.2018.06.091
13. Sengodan S, Lan R, Humphreys J, et al. Advances in reforming and partial oxidation of hydrocarbons for hydrogen production and fuel cell applications. *Renew. Sustain. Energy Rev.* 2018;82:761-780. doi:10.1016/j.rser.2017.09.071
14. Christian Enger B, Lødeng R, Holmen A. A review of catalytic partial oxidation of methane to synthesis gas with emphasis on reaction mechanisms over transition metal catalysts. *Appl. Catal. A Gen.* 2008;346:1-27. doi:10.1016/j.apcata.2008.05.018
15. Iulianelli A, Liguori S, Wilcox J, Basile A. Advances on methane steam reforming to produce hydrogen through membrane reactors technology: a review. *Catal. Rev. Sci. Eng.* 2016;58:1-35. doi:10.1080/01614940.2015.1099882
16. Oertel M, Schmitz J, Weirich W, Jendryssek-Neumann D, Schulten R. Steam reforming of natural gas with intergrated hydrogen separation for hydrogen production. *Chem. Eng. Technol.* 1987;10:248-255. doi:10.1002/ceat.270100130
17. Haryanto A, Fernando S, Murali N, Adhikari S. Current status of hydrogen production techniques by steam reforming of ethanol: a review. *Energy Fuels.* 2005;19:2098-2106. doi:10.1021/ef0500538
18. Levalley TL, Richard AR, Fan M. The progress in water gas shift and steam reforming hydrogen production technologies - a review. *Int. J. Hydrogen Energy.* 2014;39:16983-17000. doi:10.1016/j.ijhydene.2014.08.041
19. Larentis AL, De Resende NS, Salim VMM, Pinto JC. Modeling and optimization of the combined carbon dioxide reforming and partial oxidation of natural gas. *Appl. Catal. A Gen.* 2001;215:211-224. doi:10.1016/S0926-860X(01)00533-6
20. Amin NAS, Yaw TC. Thermodynamic equilibrium analysis of combined carbon dioxide reforming with partial oxidation of methane to syngas. *Int. J. Hydrogen Energy.* 2007;32:1789-1798. doi:10.1016/j.ijhydene.2006.12.004
21. Papadias D, Lee SHD, Chmielewski DJ. Autothermal reforming of gasoline for fuel cell applications: a transient reactor model. *Ind. Eng. Chem. Res.* 2006;45:5841-5858. doi:10.1021/ie051291t
22. Ahmed S, Krumpelt M. Hydrogen from hydrocarbon fuels for fuel cells. *Int. J. Hydrogen Energy.* 2001;26:291-301. doi:10.1016/S0360-3199(00)00097-5
23. Yoon S, Kang I, Bae J. Effects of ethylene on carbon formation in diesel autothermal reforming. *Int. J. Hydrogen Energy.* 2008;33:4780-4788. doi:10.1016/j.ijhydene.2008.05.025
24. Lin L, Wu L, Sui L, He S. Autothermal reforming of diesel to hydrogen and activity evaluation. *Energy Fuels.* 2018;32:7971-7977. doi:10.1021/acs.energyfuels.8b01431
25. Mohammad ZN, Rowshanzamir S, Eikani MH. Autothermal reforming of methane to synthesis gas: modeling and simulation. *Int. J. Hydrogen Energy.* 2009;34:1292-1300. doi:10.1016/j.ijhydene.2008.11.091
26. Gawade PV, Patel D, Lipscomb GG, Abraham MA. Kinetics and modeling of the flexible fuel reformer: N-hexadecane steam reforming and combustion. *Ind. Eng. Chem. Res.* 2010;49:6931-6940. doi:10.1021/ie901819x

27. Fazeli A, Behnam M. CFD modeling of methane autothermal reforming in a catalytic microreactor. *Int. J. Chem. React. Eng.* 2007;5:1-14. doi:10.2202/1542-6580.1596
28. Malik FR, Kim YB. Autothermal reforming of n-hexadecane over Rh catalyst to produce syngas in microchannel reactor using finite element method. *Int. J. Energy Res.* 2019;43:779-790. doi:10.1002/er.4308
29. Shi L, Bayless DJ, Prudich ME. A CFD model of autothermal reforming. *Int. J. Hydrogen Energy.* 2009;34:7666-7675. doi:10.1016/j.ijhydene.2009.07.039
30. Liu DJ, Kaun TD, Liao HK, Ahmed S. Characterization of kilowatt-scale autothermal reformer for production of hydrogen from heavy hydrocarbons. *Int. J. Hydrogen Energy.* 2004;29:1035-1046. doi:10.1016/j.ijhydene.2003.11.009
31. Kim D, Choi S, Jeong S, et al. Kinetic modeling of diesel autothermal reforming for fuel cell auxiliary power units. *Chem. Eng. J.* 2021;424:130564. doi:10.1016/j.cej.2021.130564
32. Brown LF. A Comparative Study of Fuels for on-Board Hydrogen Production for Fuel-Cell-Powered Automobiles. *Int J Hydrogen Energy*. 2001;26:381-397.
33. G. Kolb, IMM Compact Diesel Reformer - Hydrogen Supply for Mobility, (2021) 1-2. https://www.hannovermesse.de/apollo/hannover_messe_2021/obs/Binary/A1089088/IMM_PB_Compact_Diesel_Reformer_Hydrogen_Supply_for_Mobility.pdf.
34. Qi A, Wang S, Ni C, Wu D. Autothermal reforming of gasoline on Rh-based monolithic catalysts. *Int. J. Hydrogen Energy.* 2007;32:981-991. doi:10.1016/j.ijhydene.2006.06.072
35. Potemkin DI, Rogozhnikov VN, Ruban NV, Shilov VA. ScienceDirect comparative study of gasoline, diesel and biodiesel autothermal reforming over Rh-based FeCrAl-supported composite catalyst. *Int. J. Hydrogen Energy.* 2020;45:26197-26205. doi:10.1016/j.ijhydene.2020.01.076
36. Hla SS, Park D, Duffy GJ, et al. Kinetics of high-temperature water-gas shift reaction over two iron-based commercial catalysts using simulated coal-derived syngases. *Chem. Eng. J.* 2009;146:148-154. doi:10.1016/j.cej.2008.09.023
37. Germani G, Shuurman Y. Water-gas shift reaction kinetics over μ-structured Pt/CeO2/Al2O3 catalysts. *AIChE J.* 2006;52:1806-1813. doi:10.1002/aic

SUPPORTING INFORMATION

Additional supporting information can be found online in the Supporting Information section at the end of this article.

How to cite this article: Ješić D, Erklavec Zajec V, Bajec D, Dolanc G, Berčič G, Likozar B. Computational investigation of auto-thermal reforming process of diesel for production of hydrogen for PEM fuel cell applications. *Int J Energy Res*. 2022;1-16. doi:10.1002/er.8370